The Journal of Experimental Biology 214, 1867-1873

doi:10.1242/jeb.051342

RESEARCH ARTICLE

Aerodynamics of tip-reversal upstroke in a revolving pigeon wing

Kristen E. Crandell* and Bret W. Tobalske

Field Research Station at Fort Missoula, Division of Biological Sciences, University of Montana, Missoula, MT 59812, USA

*Author for correspondence (kristen.crandell@umontana.edu)

Accepted 28 February 2011

SUMMARY

During slow flight, bird species vary in their upstroke kinematics using either a 'flexed wing' or a distally supinated 'tip-reversal' upstroke. Two hypotheses have been presented concerning the function of the tip-reversal upstroke. The first is that this behavior is aerodynamically inactive and serves to minimize drag. The second is that the tip-reversal upstroke is capable of producing significant aerodynamic forces. Here, we explored the aerodynamic capabilities of the tip-reversal upstroke using a well-established propeller method. Rock dove (*Columba livia, N*=3) wings were spread and dried in postures characteristic of either mid-upstroke or mid-downstroke and spun at *in vivo* Reynolds numbers to simulate forces experienced during slow flight. We compared 3D wing shape for the propeller and *in vivo* kinematics, and found reasonable kinematic agreement between methods (mean differences 6.4% of wing length). We found that the wing in the upstroke posture is capable of producing substantial aerodynamic forces. At *in vivo* angles of attack (66 deg at mid-upstroke, 46 deg at mid-downstroke), the upstroke wings averaged for three birds produced a lift-to-drag ratio of 0.91, and the downstroke wings produced a lift-to-drag ratio of 3.33. Peak lift-to-drag ratio was 2.5 for upstroke and 6.3 for downstroke. Our estimates of total force production during each half-stroke suggest that downstroke produces a force that supports 115% of bodyweight, and during upstroke a forward-directed force (thrust) is produced at 36% of body weight.

Key words: upstroke, propeller model, pigeon, *Columba livia*, flight, wing, lift, drag, tip-reversal.

INTRODUCTION

In almost all birds flight plays a crucial role in survival, whether in foraging, attracting mates, defending territories, migrating or avoiding predators. In order to accomplish all of these tasks in flight, birds must first take off and accelerate to the appropriate speed. During this acceleration, flying birds appear to have two unique patterns of wing kinematics, associated with wing morphology. The first group fully flexes their wings on the upstroke and has low aspect ratio, rounded wings. The second group uses a 'tip-reversal' upstroke, in which the distal wing is heavily supinated, and includes birds with high aspect ratio, pointed wingtips (Brown, 1963; Tobalske, 2000; Tobalske et al., 2003). A notable exception to this pattern is seen in a group of birds designed for explosive take-off, *Phasianidae*, which have rounded, low aspect ratio wings but a prominent tip-reversal upstroke (Tobalske and Dial, 2000).

The functional significance of the tip-reversal upstroke has been debated for nearly a century. Early flow-visualization evidence suggested that the tip-reversal upstroke is aerodynamically inactive, meaning that it does not produce lift for weight support or thrust (Spedding et al., 1984; Spedding, 1986). However, this is unlikely given dramatic differences in wing kinematics (Brown, 1953; Tobalske and Dial, 1996) between upstroke styles, and observed increases in body acceleration during the upstroke (Brown, 1963; Aldridge, 1987). These early measures of body acceleration do not account for wing inertia in calculating center of mass acceleration, and thus may not accurately reflect performance. Recent evidence for an active upstroke is found in feather loading during the upstroke, indicating a net force directed anteriorly to the bird (Corning and Biewener, 1998), and significant differential pressure on the surfaces of the wing during upstroke through take-off and landing (Usherwood et al., 2005). Similarly, an analysis of instantaneous force changes as measured by accelerometers indicates that the tip-reversal upstroke in a cockatiel (*Nymphicus hollandicus*) provides 14% the lift of downstroke (Hedrick et al., 2004). If the upstroke provides a portion of the lift or thrust forces necessary for flight, birds that exhibit a tip-reversal upstroke may have a large advantage during slow flight in comparison to birds that flex their wings on the upstroke. Slow flight is energetically costly (Rayner, 1995); induced drag is high, so much of the power required to fly slowly is used to support the animal's weight (Ellington, 1991). Thus, we expect that animals should capitalize on mechanisms that allow them to rapidly accelerate to speeds that require less power output. Therefore, we predict that a tip-reversal upstroke will be aerodynamically active.

Here, we tested for an aerodynamic function of the upstroke in the rock dove (*Columba livia*, Gmelin 1789, hereafter 'pigeon') using a well-established propeller method (Usherwood and Ellington, 2002a; Usherwood and Ellington, 2002b) that has thus far only been used to model wing function during mid-downstroke (Usherwood and Ellington, 2002a; Usherwood and Ellington, 2002b; Altshuler et al., 2004; Usherwood, 2009). We used *in vivo* kinematics to model the posture of spread wings and to determine the Reynolds number estimated from wingtip angular velocity. We then directly measured lift and drag by mounting the dried-wing propellers on a force plate.

MATERIALS AND METHODS

Kinematics

A captive-bred pigeon was housed in an outdoor aviary at the Field Research Station at Fort Missoula. The bird was trained to fly

between horizontal platforms positioned approximately 2 m apart. Prior to kinematic recordings, the bird was marked with black permanent marker at the shoulder, wrist and each primary feather tip, and at three locations on the ventral surface of the body for later digitization. All care and experimental procedures were approved by the University of Montana IACUC.

We recorded the flight of the pigeon using four high-speed cameras: one Photron SA-3 (Photron USA Inc., San Diego, CA, USA), two Photron 1024 PCI and one Fastec Troubleshooter (Fastec Imaging, San Diego, CA, USA), synchronized using a transistor–transistor logic (TTL)-pulse. One camera was placed dorsally and behind the flight path, two were ventrally placed behind and in front of the flight path, and a fourth was placed horizontal to the bird in front of the flight path. Video recordings were made at 1000 Hz with a shutter speed of 1/10,000 s.

To analyze the kinematic data, we recorded a 36-point calibration volume (approximately 30×45×80 cm) for the space between the platforms. A direct linear transformation converted the four camera views into 3D coordinates (MATLAB R2010a, The MathWorks Inc., Natick, MA, USA) (Hedrick, 2008). Markers along the wings were digitized from recorded images to obtain 3D wing kinematics. The third wingbeat cycle following take-off was used.

We performed subsequent analysis using custom scripts in MATLAB. Angular velocity (rad s^{-1}) of the hand wing was calculated by determining a central position in three dimensions between the wrist, the 10th primary feather and the 1st secondary feather, to represent the total hand wing. We then determined the velocity vector of the hand wing, relative to the shoulder of the bird. To determine the angle of attack (α, deg) in global coordinates (accounting for translation), we measured the angle between the velocity vector of the hand wing and the vector normal to the hand-wing plane, and subtracted this from 90 deg.

Morphology

Wings were removed from three deceased birds (body mass, 446±69 g) and dried in a low temperature oven at 40°C for 1 week. We obtained paired models for each individual, with one wing in mid-upstroke posture and the other in mid-downstroke posture. Each wing was mounted on a brass rod at the proximal edge of the head of the humerus to create a one-blade propeller, with the rod acting as a counterweight (Fig. 1). Wings were photographed and analyzed in ImageJ (v1.43u, National Institutes of Health, Bethesda, MA, USA) and MATLAB to determine wing length and the first, second and third moments of area [following Usherwood and Ellington (Usherwood and Ellington, 2002b)] (Table 1). The second moment of area directly correlates with aerodynamic force, and the third moment with torque (Weis-Fogh, 1973). Thus, these two measurements allow us to account for slight differences in wing shape between birds when calculating mean vertical and horizontal forces (Eqns 1 and 2).

Propeller

Each wing was spun once at each angle of attack (α), in increments of approximately 10 deg from –10 to 90 deg. Wings were mounted to a brushless DC motor (NEMA 34 motor, Anaheim Automation Inc., Anaheim, CA, USA), and controlled with an Anaheim Automation driver and power supply (DCL 601USB, MBC 12101 and PSA 40V8A), with SMC60WIN software (v. 2.01). Revolutions per minute (r.p.m.) values were based on the mean angular velocity of the wingtip during the middle third of each half-stroke, as determined from *in vivo* kinematics for upstroke and downstroke. The third wingbeat following take-off of the live pigeon had an angular velocity of 69 rad s^{-1} for the mid-third of downstroke, and 96 rad s^{-1} for the mid-third of upstroke, which translated into 376 and 572 r.p.m., respectively.

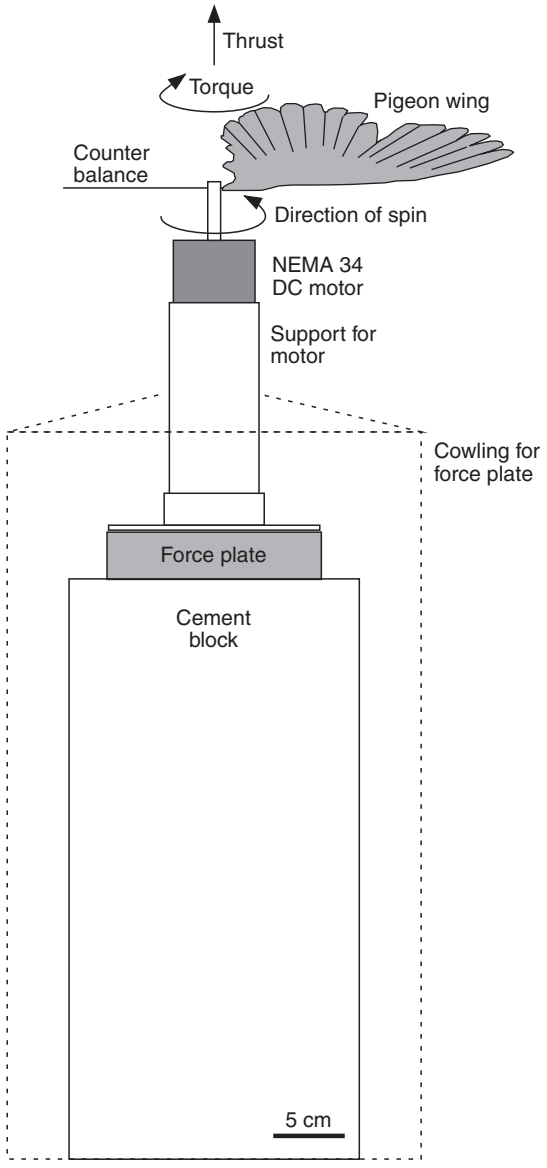

Fig. 1. The propeller setup.

The propeller shaft was constructed to allow the insertion and manipulation of the brass rod for easy rotation of the wing over a full range of α. We measured α as the acute angle between horizontal and a line described by two points on the wing: midway between the wrist, tip of the 10th primary feather and the tip of the 1st primary feather. We visualized these points using a digital video camera (Photron SA-3 using PFV 3.1.8 software) that was placed horizontal to the wing. We measured α before spinning the wing and during rotation, both to account for deformation due to aerodynamic loading of the wing and to report active α for final analysis. Active α was on average 2±3 deg less than static α.

The wings were mounted so that induced velocities in the wake would generally be directed upwards, away from the force plate. For the downstroke posture, for example, this meant the wing was mounted with its ventral surface facing upwards when α>0 deg. For

upstroke posture wings, the secondaries contacted the motor when $\alpha<50$ deg, so we oriented the wing so that the ventral surface faced downwards. The aerodynamic contributions of the counterweight were accounted for by spinning a rod with double the length of the counterweight, centered on the propeller shaft, at appropriate r.p.m. The resulting measurements were halved and subtracted from observed wing values.

We used a custom-built force plate (15×15 cm, Bertec Corp., Columbus, OH, USA) to measure vertical force along the *z*-axis and torque about the *z*-axis due to drag (Usherwood, 2009). The force plate featured a known conversion of 10,000 mN V^{-1} for force and 800 mN V^{-1} for torque. Voltage output from the force plate was converted and amplified with a digital gain of 5× using a Bertec model M6810 amplifier. We imported these data to a computer using an ADInstruments PowerLab 8SP A/D converter sampling at 1000 Hz and Chart v5.2 software using a 1 Hz low-pass digital filter (ADInstruments Inc., Colorado Springs, CO, USA). A cardboard cowling (shield) surrounded the base of the motor and the force plate in order to isolate the force plate from air velocities induced by the spinning wings (Fig. 1).

Wing shape during spinning *versus* flight

To compare deflection of primary feathers during model rotation with *in vivo* wing shape, we used 3D video recording and analysis on the propeller model (see 'Kinematics', above). We videotaped the upstroke and downstroke wing models when spinning with α comparable to *in vivo* measurements (66 deg for upstroke, 46 deg for downstroke wings). To compare wing shape between the live bird and propeller, digitized points were standardized to a right-hand rule, local coordinate system rooted at the wrist, with the *x*-axis extending through the 10th primary feather. Conversion from global to local coordinates was accomplished using a series of Euler angle transformations.

We assessed variation for each feather between a model wing (Fig. 2, blue lines) and live animal (red lines) in both the proximal–distal and ventral–dorsal axes. Feather offset was measured as the linear distance in three dimensions from each primary feather tip to its corresponding feather in the live bird, and normalized by dividing by the wing length (Fig. 2). Feathers in upstroke-postured wings differed from *in vivo* feathers by 1.96±0.97 cm or 6.05±2.75% of wing length. Downstroke posture wings differed by 2.02±0.91 cm or 6.78±3.06% of wing length.

Determining coefficients of lift and drag

Data from the force plate were converted to the coefficient of lift or drag by a series of equations presented by Usherwood and Ellington (Usherwood and Ellington, 2002a). The mean vertical force reported by the force plate ($\mathbf{F}_v$, mN) was converted to the mean vertical force coefficient (C_v):

$$C_v = \frac{2\mathbf{F}_v}{\rho S_2 \Omega^2}\ , \qquad (1)$$

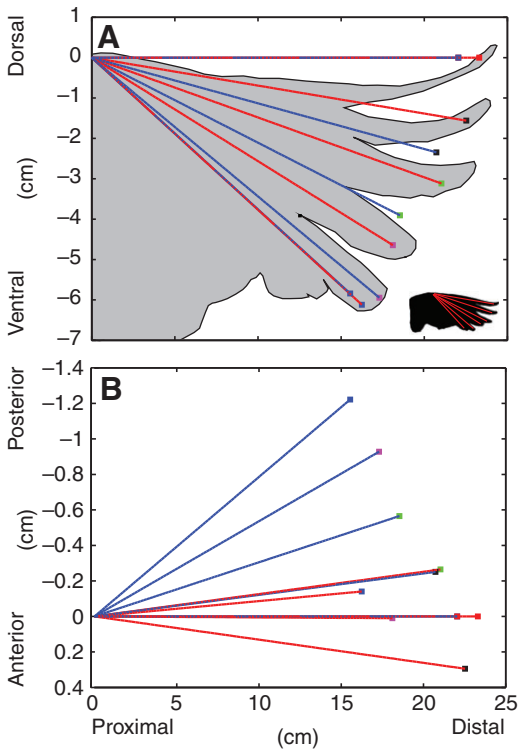

Fig. 2. A comparison of *in vivo* and propeller wing feather deflection at a 66 deg angle of attack for a wing during mid-upstroke. Live bird and propeller data were normalized to a standard coordinate system along the 10th primary feather. Each line represents a position vector from the wrist base to the tip of each primary feather (colored squares). The live bird is shown in red, the upstroke wing model from one bird in blue.
(A) Proximal–distal and ventral–dorsal axis, with feather outlines in gray.
(B) Proximal–distal and anterior–posterior axis.

where ρ is the air density (1.07 kg m^{-3}, in Missoula, MT, USA) during the experiments, S_2 is the second moment of area (Table 1) and Ω is the angular velocity (rad s^{-1}). Then, we converted the mean torque (Q, mN m) about the *z*-axis of the plate to a horizontal force coefficient (C_h):

$$C_h = \frac{2Q}{\rho S_3 \Omega^2}\ , \qquad (2)$$

where S_3 is the third moment of area.

Using both of these values, we determined the dimensionless coefficient of lift (C_L) and drag (C_D), using a value for the local downwash angle (ε) determined geometrically assuming a triangular distribution of induced velocity along the wing (Usherwood and Ellington, 2002a). This distribution has been confirmed for the

Table 1. Morphometrics for pigeon (*Columba livia*) wings used for propeller model (*N*=3)

	Downstroke	Upstroke
Wing length (*R*; m)	3.14E–01±2.47E–02	2.43E–01±1.09E–02
Wing Area (*S*; m^2)	3.35E–02±4.02E–03	2.05E–02±2.92E–03
Second moment of wing area (S_2; m^4)	8.37E–04±3.22E–04	2.36E–04±2.21E–05
Third moment of wing area (S_3; m^5)	1.76E–04±8.07E–05	3.54E–05±3.66E–06

For each bird, the right wing was positioned in upstroke posture, the left in downstroke.

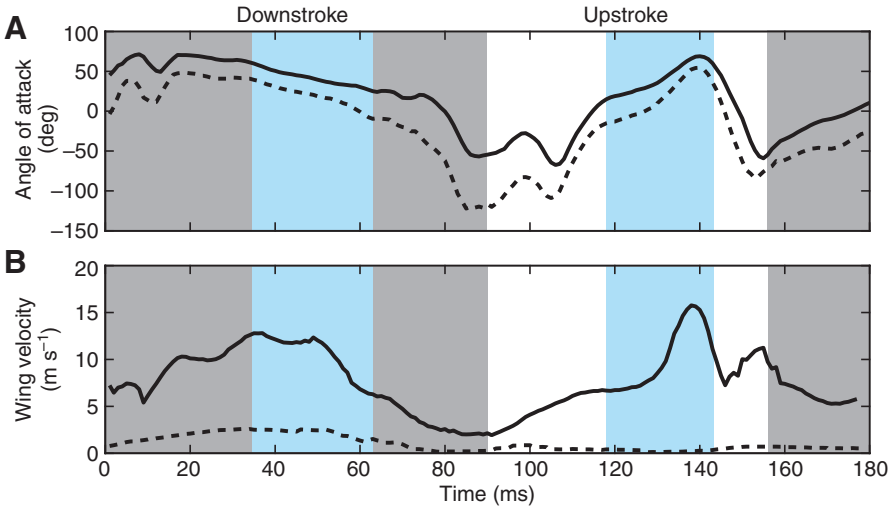

Fig. 3. Kinematic parameters extracted from the third wingbeat cycle; downstroke is shaded, and times approximated by the propeller model are highlighted in blue. (A) Geometric angle of attack (α, deg): α is shown by the solid line, α accounting for the estimated induced velocity is shown by the dashed line (see Discussion). (B) Wing velocity ($m\,s^{-1}$) for a full wingbeat cycle: wingtip is shown by the solid line, wrist is shown by the dashed line.

propeller model with chukar partridge (*Alectoris chukar*) wings using particle image velocimetry (PIV) (Heers et al., 2011). Thus, C_L was:

$$C_L = (C_v\cos\varepsilon + C_h\sin\varepsilon)\,(\cos\varepsilon)^{-2} \quad (3)$$

and C_D was:

$$C_D = (C_h\cos\varepsilon - C_v\sin\varepsilon)\,(\cos\varepsilon)^{-2}\,. \quad (4)$$

While *in vivo* upstroke kinematics qualitatively differ from downstroke kinematics, the tip-reversal upstroke rotates around the wrist, where the pigeon averages an angular velocity of only $6.5\,rad\,s^{-1}$. Thus, by positioning the wrist over the axis of rotation in our propeller model, we can assume a constant angular velocity along the hand wing during upstroke, and use the above calculations for both upstroke and downstroke wings.

Estimating *in vivo* performance

Combining *in vivo* kinematics with force coefficients extracted from the propeller model allows us to consider the force production of a pigeon during the third wingbeat cycle following take-off using coefficients measured with the propeller. First, assuming a hovering case, we can calculate lift (**L**) as:

$$\mathbf{L} = \tfrac{1}{2}\rho V^2 C_L S_2 \quad (5)$$

and drag (**D**) as:

$$\mathbf{D} = \tfrac{1}{2}\rho V^2 C_D S_2\,; \quad (6)$$

then, the resultant force ($\mathbf{F_R}$) is calculated as:

$$\mathbf{F_R} = \sqrt{(\mathbf{L}^2 + \mathbf{D}^2)}\,. \quad (7)$$

However, because the bird is moving forward, we must account for both translational velocity (Dickinson and Dickinson, 2004) and Ω along the wing (Ω_r). We used a blade element analysis (Osborne, 1951) and expanded Eqn 1 to find the vertical force ($\mathbf{F_v}$):

$$\mathbf{F_v} = \rho C_v \int_{r=0}^{R} (\Omega_r\, r + V_T)^2\, c_r\, dr\,, \quad (8)$$

where c is the chord length and V_T is the translational velocity of the wing accounting for stroke plane angle. We estimated Ω_r directly from kinematic data by dividing the leading edge (defined by a line between shoulder, wrist, and wingtip) into equal segments and taking the Ω_r for mean mid-stroke. Wing velocity increased toward the distal wingtip (Fig. 3B, wrist and wingtip). For upstroke, these calculations considered only the hand wing, as the proximal wing is flexed near the body with a low velocity (Fig. 3B, dashed line), and thus was assumed to be aerodynamically inactive. We substituted C_h for C_v in Eqn 8 to estimate $\mathbf{F_h}$. The resultant of these forces then estimates net force production.

Data analysis

We computed polars of mean C_L among the three birds sampled as a function of mean C_D as well as mean lift-to-drag ratio (C_L:C_D) as a function of α. To accomplish this, we first interpolated 95 points for C_L and C_D, to account for subtle differences in α measured between wing samples. We calculated between α=–10 deg and α=85 deg using IGOR Pro (v. 6.01, Wavemetrics, Inc., Beaverton, OR, USA). We then computed a mean and standard deviation among birds for each point in the interpolated series. Herein, we report these means ± s.d.

RESULTS

Kinematics

The third wingbeat cycle following take-off was used in analyses. Angle of attack (Fig. 3A) ranged from 72 deg at the start of downstroke to –68 deg during upstroke. Mean downstroke α=48 deg, and during the mid-third of downstroke (Fig. 3A, blue) mean α=46 deg. Mean upstroke α=–2 deg, but it ranged from –68 to 71 deg. The mean α during the mid-third of upstroke (Fig. 3A, blue) was α=66 deg. Angular velocity (Ω) for the mid-third of downstroke was $69\,rad\,s^{-1}$, and for the mid-third of upstroke Ω=$96\,rad\,s^{-1}$. Tangential velocity of the wingtip varied throughout the stroke cycle, averaging $10.1\,m\,s^{-1}$ for mid-downstroke and $8.9\,m\,s^{-1}$ for upstroke (Fig. 3B). Maximum wingtip velocity for downstroke was $12.8\,m\,s^{-1}$; for upstroke it was $15.3\,m\,s^{-1}$. Velocities along the wing measured from proximal to distal grew to a maximum at the wingtip (Fig. 3B, wrist and wingtip). However, during upstroke the proximal wing velocity remained low, likely due to being flexed against the body.

Propeller force coefficients

Coefficients for lift and drag plotted against α for all three birds revealed substantial lift production by the upstroke wings, with a general pattern that followed that of downstroke (Fig. 4). Upstroke-posture wings had a maximum C_L of 1.42±0.08 at α=53.8 deg (Fig. 4A), and downstroke wings had a maximum C_L of 1.77±0.43 at α=60.8 deg (Fig. 4C). For upstroke wings, the minimum mean

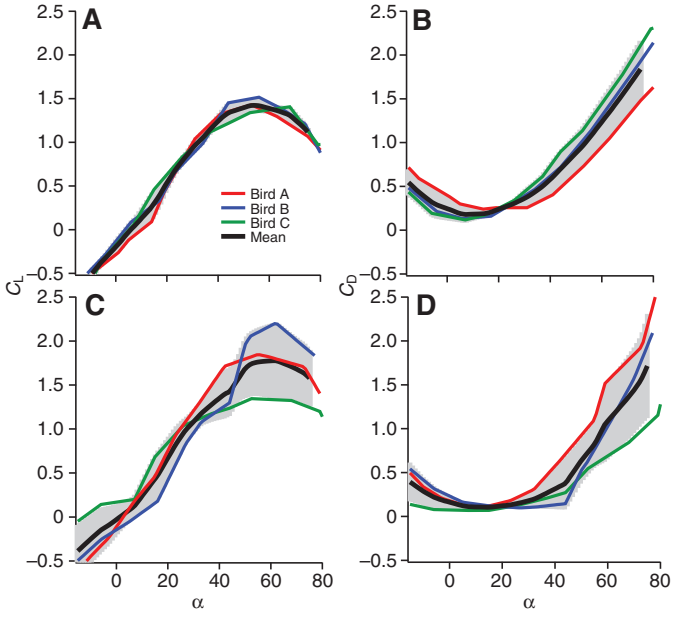

Fig. 4. Aerodynamic force coefficients for wing in upstroke (A,B) and downstroke (C,D) postures with reference to angle of attack (α). *N*=3 birds. Mean among birds is shown by the bold black line, and the shaded area represents ±s.d.

C_D was 0.18±0.09 at α=7.3 deg (Fig. 4B) while for downstroke wings mean C_D was 0.10±0.03 at α=14.3 deg (Fig. 4D).

A diagram of C_L as a function of C_D revealed that the shape of the C_L:C_D polars was similar between wing postures (Fig. 5A). The difference in values appears to caused by both a lower C_L and a higher C_D for upstroke wings, due to the minimum and maximum values seen in Fig. 4. The slopes of the C_L:C_D polar for upstroke and downstroke wings are almost identical (Fig. 5A), as evidenced by the similar α at the maximum C_L:C_D (Fig. 5B). The maximum C_L:C_D for wings in downstroke posture was 6.3, which occurred at α=26.5 deg. Wings in upstroke posture had a lower maximum C_L:C_D of 2.5, at α=28.0 deg. At measured *in vivo* α=66 deg during mid-upstroke, the C_L:C_D is approximately 0.91. At this α, C_L=1.33 and C_D=1.46. The C_L:C_D for downstroke posture was 3.33 at the *in vivo* α=46 deg, with C_L=1.54 and C_D=0.49.

Bracketing *in vivo* performance

Various assumptions provided alternative estimates for *in vivo* force production. We observed minimum values for lift and drag if we assumed a bird was hovering, with no forward translational velocity (Eqns 5 and 6). In this instance, the bird (4.37 N) would produce a resultant force ($\mathbf{F_R}$) of 51.3% body weight (2.24 N) with both wings during mid-downstroke (α=46 deg). During mid-upstroke (α=66 deg), the pigeon could produce a $\mathbf{F_R}$ of 107% body weight (4.71 N).

However, these values likely do not represent *in vivo* performance: during the third wingbeat following take-off, the bird has already reached a forward velocity of 2.9 m s^{-1}. When including this translation in our estimation by incorporating translational velocity (V_T) in a blade-element analysis (Eqn 8), mid-downstroke $\mathbf{F_R}$ produces 8.7 N, 198% of body weight. With a stroke plane angle of 38 deg during downstroke, the $\mathbf{F_R}$ is directed in front of the bird but near vertical, at 71 deg from the global horizontal plane, thus providing mostly weight support. During mid-upstroke, $\mathbf{F_R}$=5.43 N, 124% body weight. The upstroke stroke plane angle is 21 deg, and

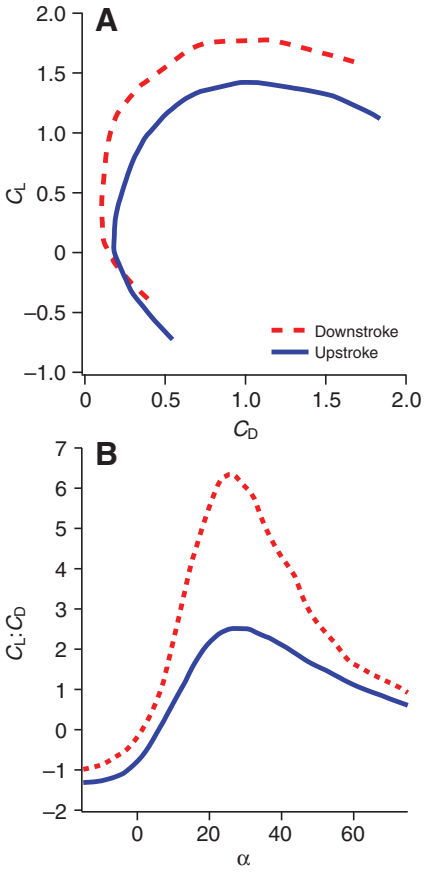

Fig. 5. (A) Polar diagram showing mean coefficient of lift (C_L) as a function of mean coefficient of drag (C_D) for *N*=3 pigeon wings. (B) Mean lift-to-drag ratio (C_L:C_D) against angle of attack (α) for *N*=3 pigeon wings.

$\mathbf{F_R}$ is oriented in front of the bird, 23 deg above the global horizontal plane, providing mostly thrust. These values probably represent extremes. Consider that mid-downstroke values appear to reflect the kinematics through the majority of downstroke (Fig. 3), while mid-upstroke kinematics reflects only a small portion of the entire half-cycle (Fig. 3). Extrapolating this calculation for the entire downstroke, which is approximately 58% of the wingbeat cycle, suggests that the bird produces a mean force of 115% body weight during downstroke. Throughout the entire upstroke, 42% of the wingbeat cycle, the mean force produced would be 36% bodyweight.

DISCUSSION

Given the debate over the functional significance of the tip-reversal upstroke (Brown, 1963; Spedding et al., 1984; Spedding, 1986; Aldridge, 1987; Hedrick et al., 2004; Tobalske et al., 2003), our most important result is that the model wings in upstroke posture produced a large amount of aerodynamic force (Figs 4 and 5). In fact, the downstroke and upstroke wings appear to perform similarly, both reaching maximum C_L:C_D at approximately α=26 deg (Fig. 5). This suggests that during mid-upstroke, significant force can be produced to help support weight or generate thrust, and the magnitude of this force is dependent on α in much the same way as for downstroke.

At *in vivo* angles of attack, we estimate the upstroke is capable of producing mean force as great as 36% body weight during this half of the stroke cycle. This value is within the range of lift produced

by an active upstroke in hovering hummingbirds (33–48%) (Warrick et al., 2005; Warrick et al., 2009). Our results are supported by measures of feather bending during slow flight. Values of strain on primary feathers during upstroke are 43% that of downstroke (Corning and Biewener, 1998), suggesting that upstroke values reported here are not unreasonable for *in vivo* performance. The upstroke force we estimated also falls near the range of 14% the lift of downstroke measured with accelerometers in cockatiels (Hedrick et al., 2004).

Aerodynamically active upstrokes have been reported in several bat species that exhibit a similar wing-tip reversal pattern. The horseshoe bat (*Rhionolophus ferrumenquinum*) has an angle of incidence at the wingtip during upstroke of 70 deg (Aldridge, 1986), close to our reported value of 66 deg. Introductory analyses of changes in acceleration found an aerodynamically active upstroke during vertical flight (Aldridge, 1987) and hovering (Aldridge, 1991) of bats. In-depth kinematic analyses accounting for inertial effects will be crucial to validate these findings. More recent analyses of the wake in slow-flying bats using PIV show a vortex ring shed at the end of upstroke (Hedenström et al., 2007; Johannson et al., 2008), indicating both thrust and weight support produced on the upstroke. Further PIV analyses show that the role of upstroke changes to only provide weight support at higher speeds in bats (Wolf et al., 2010). Our results suggest that birds exhibiting tip-reversal upstroke may use aerodynamic mechanisms similar to bats during slow flight.

Our findings indicate that slow-flying pigeons are using their wings at a lower C_L:C_D than is potentially available to them (Fig. 5A) during both upstroke and downstroke. However, they are operating at α close to, or at, maximum lift performance (Fig. 5B). Peak C_L for downstroke was 1.8 at α=61 deg, and for upstroke it was 1.4 at α=54 deg. At such high α on the upstroke, pigeons appear to be operating where lift and drag are almost equivalent (C_L:C_D=0.91). The resultant force during mid-upstroke is directed forward, 23 deg from global horizontal, due in part to high drag. This suggests that drag may play an important role during the upstroke, possibly to assist in weight support or thrust. This may also be the case for bats in slow flight (Aldridge, 1987; Norberg, 1976), and for chukar partridges during wing-assisted incline running (Tobalske and Dial, 2007).

Our propeller measurements for downstroke were consistent with previously published values for a pigeon wing in downstroke posture. Usherwood reports a maximum C_L:C_D of 5.4 for a pigeon wing spun on a propeller emulating slow flight (Usherwood, 2009), in comparison to our C_L:C_D of 6.3 (Fig. 5B). Maximum C_L for the same wings was 1.64 (Usherwood, 2009), while our value was 1.77. Our slightly higher values are potentially due to differences in wing morphology (Table 1) and spinning speed. Estimated lift and drag values for downstroke from kinematic analyses of pigeons in slow flight (Berg and Biewener, 2008) yielded values of C_L=1.44±0.29 and C_D=1.01±0.08, within the bounds of our values. Notably, the s.d. variation for C_L and C_D between wings increases with higher α in downstroke wings, but equivalent variation did not occur for upstroke wings. During slow flight, unsteady aerodynamic effects likely dominate (Ellington, 1984). At such high α, this may include periodic leading edge vorticity (Warrick et al., 2005) detachment. This flow separation may lead to unpredictable variation in both C_L and C_D throughout the half-stroke. In contrast, wings in upstroke posture, with smaller observed s.d. at high angles of attack, may reduce these effects *via* the separation of the primary feathers, allowing individual feathers to function as individual airfoils with lower α (Brown, 1963). Further exploration using flow-visualization would help tease apart differences between *in vivo* and propeller aerodynamics.

It is important to note that values reported here represent values for mid-stroke. Our estimate of *in vivo* $\mathbf{F_R}$ provide a lower bracket for downstroke of 51% bodyweight during hovering, and an upper bracket of 198% when accounting for translation (V_T). The resultants from these calculations are directed up 71 deg from global horizontal, indicating the downstroke acts to support weight. The same calculation for upstroke suggests a bracket between 107 and 124% body weight. The upstroke resultant is directed forward, 23 deg from global horizontal due to high levels of drag, suggesting upstroke provides thrust. These values likely provide a reasonable estimate for downstroke. Even then, wing velocity is greatest at mid-stroke, when our estimates are based, and resulting forces should be proportional to the square of wing velocity (Ellington, 1984). The values for upstroke are likely an over-estimate, as we applied static coefficients to a highly unsteady event. In the upstroke, α and wing velocity are highly time variant (Fig. 3), and our estimation occurred at near peak wing velocity. Moreover, wing posture appears to change more dramatically throughout the upstroke when compared with the downstroke, and it may be the mid-stroke posture that is optimal for force production. Our kinematic analysis throughout the stroke cycle (Fig. 3) illustrates that as the hand wing pronates using a rapid 'flick' at the end of upstroke, a changing α occurs, as also observed to a lesser extent in the downstroke in the pigeon (Warrick and Dial, 1998) and cockatiel (Hedrick et al., 2002). Such constant variation in wing velocity and α in upstroke is also exhibited by hovering hummingbirds, and it appears that this helps to explain variation in circulation on the wing (Tobalske et al., 2007; Warrick et al., 2009). Thus, our final estimate for net force produced during both halves of the stroke cycle, using Ω_r and accounting for the percentage of the total wingbeat cycle, is probably the most accurate for predicting pigeon performance.

Additionally, it is critical to note that the dried wing models do not accurately reflect all aspects of mid-downstroke or mid-upstroke. The preparation process, in which wings are isolated and dried, likely changes the mechanical properties of the wing. Similarly, the posture adopted by the models may not be an accurate representation of actual kinematics, as evidenced in slight differences in feather location between pigeon and propeller measurements (Fig. 2). While our model reflects the forces during an impulse, in reality the wing is morphing throughout most of the stroke cycle. For example, wing flexibility and compliance throughout a stroke significantly increases lift in insects (Mountcastle and Daniel, 2009; Young et al., 2009). During the stroke cycle of the pigeon, significant pronation and supination also occur. This results in wing camber and wing twist, which significantly improve aerodynamic forces in the locust (Young et al., 2009). The propeller model wings are probably unable to fully reflect these characteristics.

Our measure of α on the propeller is the geometric angle of attack, which does not account for induced velocity. It is likely that the angle of incidence (Vogel, 1994) was lower than our reported α. While our calculations of C_L and C_D account for local induced velocity (ε, Eqns 3 and 4), note that α is reported without accounting for local induced velocity. Thus, for example, a calculation for our mid-upstroke propeller model using a Rankine–Froude momentum jet model (Usherwood and Ellington, 2002a; Vogel, 1994) suggests that local induced velocity at the wingtip would be ~1.26 m s^{-1}. Therefore, the angle of incidence would be 52 deg, compared with 65 deg for α. To explore the possible impact of induced velocity throughout the stroke cycle, we present a simulated α throughout the stroke cycle (Fig. 3A, dotted line). This rough calculation using the same momentum jet model accounts for induced velocity during the downstroke, assuming that the induced velocity of the

downstroke heavily influences the upstroke as it returns through the downstroke wake. In general, these effects appear minimal (~10 deg), but have most pronounced effects at the downstroke–upstroke transition. Empirical measures of induced velocity would improve understanding of wing function *in vivo*, but will require methods such as PIV (Spedding and Hedenström, 2009) or hot-wire anemometry (Norberg et al., 1993).

CONCLUSIONS

The propeller, while a simplification of the wingbeat, provides new insight into the functional significance of the tip-reversal upstroke in avian flight. It has often been assumed that the tip-reversal posture in birds is simply to reduce drag by allowing air to pass through individual feathers, creating a Venetian blind effect (Brown, 1953; Brown, 1963). Thus far, hummingbirds are the only birds that are known to use an aerodynamically active upstroke during slow flight (Warrick et al., 2005). Our new measurements indicated that tip-reversal upstroke, widespread in birds with pointed wings, might be more similar to the hummingbird wingbeat than previously thought. If an aerodynamically active upstroke does offer advantages, why is it that not all birds use a tip-reversal? A future challenge will be to better understand the trade-offs that have led to many species with rounded wings using a flexed-wing upstroke.

LIST OF SYMBOLS

c	chord length
C_D	coefficient of drag
C_h	mean horizontal force coefficient
C_L	coefficient of lift
C_v	mean vertical force coefficient
$\mathbf{D}$	drag
$\mathbf{F_h}$	horizontal force
$\mathbf{F_R}$	resultant force
$\mathbf{F_v}$	vertical force
$\mathbf{L}$	lift
Q	torque about the motor
r	radial distance along the wing
R	wing length
S	wing area
S_2	second moment of area
S_3	third moment of area
V_T	wing translational velocity
α	geometric angle of attack
ε	downwash angle
ρ	air density
Ω	angular velocity

ACKNOWLEDGEMENTS

We thank Ashley Heers and Terry Dial for help with the development our propeller model and methods of data analysis. We thank Brandon Jackson, Ashley Heers, Ken Dial and two anonymous reviewers for helpful comments on a draft of this manuscript. Supported by NSF grants IOS-0923606 and IOS-0919799.

REFERENCES

Aldridge, H. D. J. N. (1986). Kinematics and aerodynamics of the greater horseshoe bat, *Rhionolophus ferrumenquinum*, in horizontal flight at various flight speeds. *J. Exp. Biol.* **126**, 479-497.
Aldridge, H. D. J. N. (1987). Body accelerations during the wingbeat in six bat species: the function of the upstroke in thrust generation, *J. Exp. Biol.* **130**, 275-293.
Aldridge, H. D. J. N. (1991). Vertical flight in the greater horseshoe bat *Rhinolophus ferrumequinum*. *J. Exp. Biol.* **157**, 183-204.
Altshuler, D. L., Dudley, R. and Ellington, C. P. (2004). Aerodynamic forces of revolving hummingbird wings and wing models. *J. Zool. Lond.* **264**, 327-332.
Berg, A. M. and Biewener, A. A. (2008). Kinematics and power requirements of ascending and descending flight in the pigeon (*Columba livia*) *J. Exp. Biol.* **211**, 1120-1130.
Brown, R. H. J. (1953). The flight of birds. II. Wing function in relation to flight speed. *J. Exp. Biol.* **30**, 90-103.
Brown, R. H. J. (1963). The flight of birds. *Biol. Rev. Camb. Philos.* **38**, 460-489.
Corning, W. R. and Biewener, A. A. (1998). *In vivo* strains in pigeon flight feather shafts: implications for structural design. *J. Exp. Biol.* **201**, 3057-3066.
Dickinson, W. B. and Dickinson, M. H. (2004). The effect of advance ratio on the aerodynamics of revolving wings. *J. Exp. Biol.* **207**, 4269-4281.
Ellington, C. P. (1984). The aerodynamics of hovering insect flight. VI. Lift and power requirements. *Philos. Trans. R. Soc. B* **305**, 145-181.
Ellington, C. P. (1991). Limitations on animal flight performance. *J. Exp. Biol.* **160**, 71-91.
Hedenström, A., Johansson, L. C., Wolf, M., von Busse, R., Winter, Y. and Spedding, G. R. (2007). Bat flight generates complex aerodynamic tracks. *Science* **316**, 894-897.
Hedrick, T. L. (2008). Software techniques for two- and three-dimensional kinematic measurements of biological and biomimetic systems. *Bioinspir. Biomim.* **3**, 034001.
Hedrick, T. L., Tobalske, B. W. and Biewener, A. A. (2002). Estimates of circulation and gait change based on a three-dimensional kinematic analysis of flight in cockatiels (*Nymphicus hollandicus*) and ringed turtle-doves (*Streptopelia risoria*). *J. Exp. Biol.* **205**, 1389-1409.
Hedrick, T. L., Usherwood, J. R. and Biewener, A. A. (2004). Wing inertia and whole-body acceleration: an analysis of instantaneous aerodynamic force production in cockatiels (*Nymphicus hollandicus*) flying across a range of speeds. *J. Exp. Biol.* **207**, 1689-1702.
Heers, A. M., Tobalske, B. W. and Dial, K. P. (2011). Ontogeny of lift and drag production in ground birds. *J. Exp. Biol.* **214**, 717-725.
Johansson, L. C., Wolf, M., vone Busse, R., Winter, Y., Spedding, G. R. and Hedenström, A. (2008). The near and far wake of Pallas' long tongued bat (*Glossophaga soricina*). *J. Exp. Biol.* **211**, 2909-2918.
Mountcastle, A. M. and Daniel, T. L. (2009). Aerodynamic and functional consequences of wing compliance. *Exp. Fluids* **46**, 873-882.
Norberg, U. M. (1976). Aerodynamics, kinematics, and energetics of horizontal flapping flight in long-eared bat (*Plecotus auritus*). *J. Exp. Biol.* **65**, 179-212.
Norberg, U. M., Kunz, T. H., Steffensen, J. F., Winter, Y. and Von Helversen, O. (1993). The cost of hovering and forward flight in a nectar-feeding bat, *Glossophaga soricina*, estimated from aerodynamic theory. *J. Exp. Biol.* **182**, 207-227.
Osborne, M. F. M. (1951). Aerodynamics of flapping flight with application to insects. *J. Exp. Biol.* **28**, 221-245.
Rayner, J. M. V. (1995). Flight mechanics and constraints on flight performance. *Israel J. Zool.* **41**, 321-342.
Spedding, G. R. (1986). The wake of a jackdaw (*Corvus monedula*) in slow flight. *J. Exp. Biol.* **125**, 287-307.
Spedding, G. R. and Hedenström, A. (2009). PIV-based investigations of animal flight. *Exp. Fluids* **46**, 749-763.
Spedding, G. R., Rayner, J. M. V. and Pennycuick, C. J. (1984). Momentum and energy in the wake of a pigeon (*Columba livia*) in slow flight. *J. Exp. Biol.* **111**, 81-102.
Tobalske, B. W. (2000). Biomechanics and physiology of gait selection in flying birds. *Phys. Biochem. Zool.* **73**, 736-750.
Tobalske, B. W. and Dial, K. P. (1996). Flight kinematics of black-billed magpies and pigeons over a wide range of speeds. *J. Exp. Biol.* **199**, 263-280.
Tobalske, B. W. and Dial, K. P. (2000). Effects of body size on take-off flight performance in the *Phasianidae* (*Aves*). *J. Exp. Biol.* **203**, 3319-3332.
Tobalske, B. W. and Dial, K. P. (2007). Aerodynamics of wing-assisted incline running in birds. *J. Exp. Biol.* **210**, 1742-1751.
Tobalske, B. W., Hedrick, T. L. and Biewener, A. A. (2003). Wing kinematics of avian flight across speeds. *J. Avian Biol.* **34**, 177-184.
Tobalske, B. W., Warrick, D. R., Clark, C. J., Powers, D. R., Hedrick, T. L., Hyder, G. A. and Biewener, A. A. (2007). Three-dimensional kinematics of hummingbird flight. *J. Exp. Biol.* **210**, 2368-2382.
Usherwood, J. R. (2009). The aerodynamic forces and pressure distribution of a revolving pigeon wing. *Exp. Fluids* **46**, 991-1003.
Usherwood, J. R. and Ellington, C. P. (2002a). The aerodynamics of revolving wings – I. Model hawkmoth wings. *J. Exp. Biol.* **205**, 1547-1564.
Usherwood, J. R. and Ellington, C. P. (2002b). The aerodynamics of revolving wings – II. Propeller force coefficients from mayfly to quail. *J. Exp. Biol.* **205**, 1565-1576.
Usherwood, J. R., Hedrick, T. L., McGowan, C. P. and Biewener, A. A. (2005). Dynamic pressure maps for wings and tails of pigeons in slow, flapping flight, and their energetic implications. *J. Exp. Biol.* **208**, 355-369.
Vogel, S. (1994). *Life in Moving Fluids: The Physical Biology of Flow.* Princeton: Princeton University Press.
Warrick, D. R. and Dial, K. P. (1998). Kinematic, aerodynamic, and anatomical mechanisms in the slow, maneuvering flight of pigeons. *J. Exp. Biol.* **201**, 655-672.
Warrick, D. R., Tobalske, B. W. and Powers, D. R. (2005). Aerodynamics of the hovering hummingbird. *Nature* **435**, 1094-1097.
Warrick, D. R., Tobalske, B. W. and Powers, D. R. (2009). Lift production in the hovering hummingbird. *Proc. R. Soc. B.* **276**, 3747-3752.
Weis-Fogh, T. (1973). Quick estimates of flight fitness in hovering animals, including novel mechanisms for lift production. *J. Exp. Biol.* **59**, 169-230.
Wolf, M., Johansson, L. C., von Busse, R., Winter, Y. and Hedenström, A. (2010). Kinematics of flight and the relationship to the vortex wake of the Pallas' long tongued bat (*Glossophaga soricina*). *J. Exp. Biol.* **213**, 2142-2153.
Young, J., Walker, S. M., Bomphrey, R. J., Taylor, G. K. and Thomas, A. L. R. (2009). Details of insect wing design and deformation enhance aerodynamic function and flight efficiency. *Science* **325**, 1549-1552.